Spontaneous Polarization Buildup in a Room-Temperature Polariton Laser

J. J. Baumberg,[1] A. V. Kavokin,[2] S. Christopoulos,[1] A. J. D. Grundy,[2] R. Butté,[3] G. Christmann,[3] D. D. Solnyshkov,[4] G. Malpuech,[4] G. Baldassarri Höger von Högersthal,[2] E. Feltin,[3] J.-F. Carlin,[3] and N. Grandjean[3]

[1]*NanoPhotonics Centre, Department of Physics, University of Cambridge, Cambridge, CB3 0HE, United Kingdom*
[2]*School of Physics and Astronomy, University of Southampton, Highfield, Southampton, SO17 1BJ, United Kingdom*
[3]*Institute of Quantum Electronics and Photonics, EPFL, 1015 Lausanne, Switzerland*
[4]*LASMEA, CNRS, University Blaise Pascal, 632177 Aubiere Cedex, France*

(Received 2 April 2008; revised manuscript received 8 August 2008; published 26 September 2008)

We observe the buildup of strong (~50%) spontaneous vector polarization in emission from a GaN-based polariton laser excited by short optical pulses at room temperature. The Stokes vector of emitted light changes its orientation randomly from one excitation pulse to another, so that the time-integrated polarization remains zero. This behavior is completely different from any previous laser. We interpret this observation in terms of the spontaneous symmetry breaking in a Bose-Einstein condensate of exciton polaritons.

DOI: 10.1103/PhysRevLett.101.136409 PACS numbers: 71.36.+c, 03.75.Kk, 73.21.−b, 81.07.−b

Polariton lasers are coherent light sources based on emission of light from a coherent ensemble of exciton polaritons—the mixed light-exciton quasiparticles in semiconductor microcavities. The concept of polariton lasing was first proposed in 1996 [1], followed a few years later by reports of coherent polariton emission in microcavities [2–4]. Recently, we reported polariton lasing at room temperature in GaN-based microcavities [5]. Apart from being very promising for applications, the concept of polariton lasing involves several fundamental physics issues. Contrary to conventional lasers, polariton lasers emit coherent and monochromatic light *spontaneously*. This is achieved when mixed light-matter quasiparticles (exciton polaritons) condense inside a semiconductor microcavity. Bose-Einstein condensation (BEC) of the polaritons is a subject of intense experimental and theoretical research at present. Several experimental works claiming polariton BEC have appeared recently [6–8]. Though polariton BEC implies polariton lasing, these two phenomena are not identical. For polariton lasing a macroscopically populated quantum state of exciton polaritons must be created, which can be considered as a polariton condensate. Polariton lasing does not require thermal equilibrium in the system or the spontaneous buildup of the order parameter, which are the main criteria for BEC when understood as a thermodynamic phase transition. Which experimental measurement should be considered as decisive proof for the exciton polariton BEC is still a subject of debate within the community. Thermalization of the exciton polaritons detected by angle-resolved photoluminescence measurements has been considered one of the key criteria for a long time [6,7]. However, a similar angular dependence of the photoluminescence has also been observed in GaAs-based photon lasers [9]. The spatial coherence of polariton emission demonstrated in Ref. [6] is characteristic for conventional lasers as well. Recent theoretical work suggests that observation of the spontaneous buildup of the vector polarization in emission from polariton lasers would be evidence for the spontaneous symmetry breaking in the system [10–12]. In turn, spontaneous symmetry breaking is considered to be a smoking gun for BEC ever since the pioneering work of Goldstone [13,14].

Here we report observations of the buildup of the spontaneous vector polarization at room temperature in bulk GaN microcavities. Unlike the recent low temperature experiments on BEC in CdTe- and GaAs-based cavities in which the polarization direction was pinned along the crystal axes [6,7], we find that the polarization of emitted light varies stochastically from one experiment to another. We also observe the thresholdlike buildup of population in the lowest energy polariton state, a Boltzmann distribution of exciton polaritons in excited states (with an effective temperature of 360 K), and the buildup of first order coherence. Thus each criterion for polariton BEC formulated in previous works is fulfilled in our sample.

Intense theoretical research on BEC from 1938 to 1965 led to the definition of the BEC criterion for a weakly interacting Bose gas which is associated with the appearance of a macroscopic condensate wave function, $\psi(\underline{r})$, forming the order parameter of the phase transition. Yang [15] termed the phenomenon "off-diagonal long-range order." The system Hamiltonian is invariant to the phase of $\psi(\underline{r})$; however, at the phase transition the symmetric solution becomes unstable. The system therefore breaks symmetry by choosing a *specific* phase that is adopted throughout the whole condensate.

In this context, BEC of exciton polaritons has important specific features: the exciton polaritons are spinor quasiparticles with two possible spin projections [up (down) corresponding to right- (left-)circular polarizations of emitted light]. Therefore, the order parameter for exciton polariton BEC possesses two components: $\psi(\underline{r}) = [\psi_\uparrow(\underline{r}) \atop \psi_\downarrow(\underline{r})]$, where $\psi_\uparrow(\underline{r})$ and $\psi_\downarrow(\underline{r})$ are the complex spin-up and spin-down wave functions, respectively. The 3D polarization

vector, **S** (termed the Stokes vector in classical optics or pseudospin in quantum mechanics), is linked to these wave functions through $S_x = \mathrm{Re}(\psi_\uparrow^* \psi_\downarrow)$, $S_y = \mathrm{Im}(\psi_\uparrow^* \psi_\downarrow)$, and $S_z = \frac{1}{2}(|\psi_\uparrow|^2 - |\psi_\downarrow|^2)$. The absolute polarization degree of the condensate is $\rho = (|\psi_\uparrow|^2 + |\psi_\downarrow|^2)/N_0$, where N_0 is the occupation number of the condensate. It is linked with linear, diagonal, and circular polarization degrees ρ_l, ρ_d, ρ_c by $\rho = \sqrt{\rho_l^2 + \rho_d^2 + \rho_c^2}$, where $\rho_{l,d,c} = 2S_{x,y,z}/N_0$. In microcavities pumped below threshold, $|\psi| = 0$, while at threshold, ψ builds up due to stimulated scattering of polaritons from the excited states to the condensate [16]. The essential feature of a *bulk* microcavity is the absence of a spin quantization axis leading to spin-isotropic polariton-polariton interactions. Extending the method of [16], the probability of realizing a given value of the order parameter at a given time $P(\psi, t)$ is described by a nonlinear Fokker-Planck equation

$$\frac{\partial P}{\partial t} = \nabla[P\nabla U(\psi, t) + D(t)\nabla P], \tag{1}$$

where the effective potential is given by

$$U = \{[W_{\mathrm{out}}(t) - W_{\mathrm{in}}(t)]|\psi|^2 + \alpha|\psi|^4\}/4, \tag{2}$$

and the diffusion coefficient $D = W_{\mathrm{in}}(t)/4$. Here $W_{\mathrm{in}}(t)$ is the rate of exciton polaritons scattering into the condensate which is dependent on the pumping strength and the coupling of the condensate to the reservoir of exciton polaritons having large wave vectors. W_{out} is the depletion rate of the condensate depending mostly on the polariton radiative lifetime, while $\alpha > 0$ is the polariton-polariton interaction constant. The population of the condensate N_0 is linked to W_{in} and W_{out} via the Boltzmann equation

$$\frac{dN_0}{dt} = W_{\mathrm{in}}(t)(N_0 + 1) - W_{\mathrm{out}}(t)N_0. \tag{3}$$

Above threshold, $W_{\mathrm{in}} > W_{\mathrm{out}}$ so that the potential (2) has a maximum at $|\psi| = 0$ surrounded by a circular minimum at finite $|\psi|$. This allows for an efficient diffusion of the order parameter out of the center of the effective potential. The buildup of this order parameter explicitly results in a polarization buildup. The resulting value of the absolute polarization is linked to the minimum of the effective potential (2), which has no privileged polarization, so that in each experiment the system chooses its polarization randomly. Once formed, the polarization continues changing slowly due to the diffusion of the order parameter within the effective potential.

To demonstrate experimentally the buildup of polariton vector polarization, we have grown a crack-free GaN-based microcavity, where the excitons are stable at 300 K due to their large binding energy. To avoid polarization pinning which is likely to be inevitable in quantum well cavities due to their reduced symmetry, the cavity is composed of bulk GaN. In this semiconductor, the different types of excitons are mixed and the exciton-exciton interaction is expected to be spin-isotropic [17] so that polariton BEC in such cavities should be accompanied by the spontaneous appearance of completely arbitrary polarization. This device structure demonstrates strong exciton-photon coupling and polariton lasing at room temperature as we showed recently [5]. We briefly describe the sample and experiment which is fully characterized in Ref. [5] and references therein. Lattice-matched AlInN/AlGaN bottom and SiO_2/Si_3N_4 top Bragg reflectors are used to sandwich a 220 nm-thick GaN active layer, forming a microcavity in the strong coupling regime displaying the classic exciton polariton anticrossing dispersion with angle in ultraviolet emission near $\lambda = 365$ nm with a Rabi splitting of 36 meV. The detuning varies nonmonotonically across the sample and is negatively detuned (by <30 meV) for results reported here (but the results are not strongly detuning-dependent). The sample is pumped at an angle of 30° with 150 fs nonresonant UV pulses tuned to 300 nm where the top mirror becomes transparent. The experimental excitation is repeated every 4.2 μs, and the emission spectra, angle dependence, and polarization are recorded using UV-sensitive CCDs and photomultipliers (PMTs). The cone of emitted light in k space (where k is the in-plane wave vector) is shown in Figs. 1(a) and 1(b) both below and above the threshold $I_{\mathrm{th}} \sim 1.0$ mW, showing the emergence of macroscopic occupation near $k = 0$. The exponential increase of light emission from polaritons in-

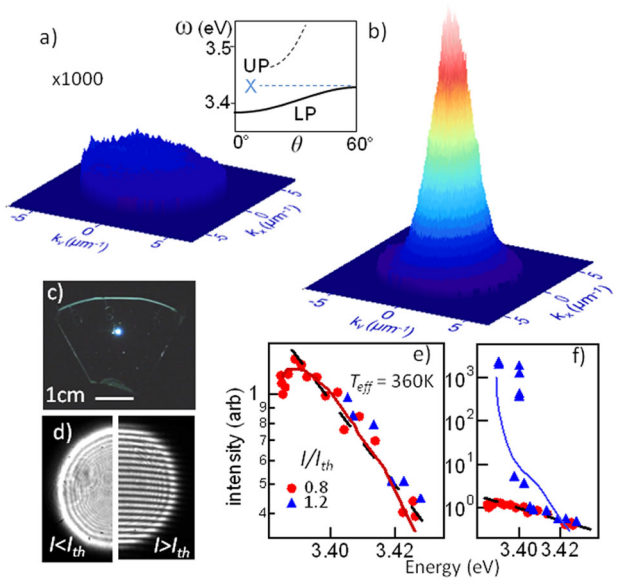

FIG. 1 (color online). Formation of polariton lasing at $T = 300$ K in a GaN microcavity at in-plane wave vectors up to $k_{\mathrm{max}} = 7\ \mu\mathrm{m}^{-1}$ for (a) just below (scaled up by $\times 1000$) and (b) just above threshold ($I_{\mathrm{th}} \sim 1$ mW). Inset shows dispersion. (c) Image of pumped sample above threshold. (d) Interference of far-field emission cone through a slightly misaligned Michelson interferometer above and below threshold. (e),(f) Polariton emission intensity just below and above threshold as a function of energy, together with Boltzmann fit (dashed line) giving an effective temperature of 360 K, and result from kinetic simulation (solid lines).

side the microcavity at threshold manifests polariton lasing [Fig. 1(c)].

We interfere two copies of the collimated far-field light cone in a Michelson interferometer to display the first order coherence [Fig. 1(d)]. The temporal decay of this coherence is dominated by the subpicosecond emission time of the condensate. Just below threshold, the integrated polariton emission measured at each angle follows a quasithermal Boltzmann-like distribution with an effective temperature of $\simeq 360 \pm 30$ K [Fig. 1(e)] [18]. Similar results are obtained across the wafer, with variation mainly due to the local quality factor of the cavity mode [19].

The time-integrated polarization of emission we observe is exactly zero, independent of the orientation of the analyzer axes. To resolve the polarization of the emission for each experimental realization of the condensation from each excitation pulse, we polarization split the emission and focus both orthogonal components either (a) onto the input slit of a streak camera operated in single-shot mode or (b) onto the cathodes of balanced PMTs. Previous experiments have shown the maximum lifetime of electronic excitations in the sample is 35 ps (with an exponential decay time). Hence between pulses the sample completely recovers, and each pulse forms a new experiment. Light emerging up to $\pm 15°$ to the sample normal is collected using a UV achromatic lens and collimated. The light passes through broadband UV wave plates (half wave and quarter wave) before being split by polarization beam splitters (care has to be taken over the angular acceptance and alignment of these optics). In the experiments which use repeated measurements of one particular polarization basis, a single polarization beam splitter is used, and the two emerging beams are individually focused on two detectors. For streak camera measurements, they are focused onto different positions on the input slit of the streak camera, and their optical paths made equal so that the two polarization components of each pulse appear at the same time position on the streak image. The streak camera is manually triggered, with a gain sufficient to record the relatively weak emission, allowing extraction of each polarization component averaged over each laser shot. Equivalently, we also use UV-sensitive photomultipliers instead of the streak camera, with a temporal response of <100 ns, and after preamplification and pulse cleanup electronics, these are converted on a computer card with sample-and-hole facility which records simultaneous measurements on all channels. The overall time resolution of the system is <1 μs, and allows extraction of the intensity of each polarization component for each pulse, over thousands of successive shots (Fig. 2). We always use the wave plates to swap the polarization basis between PMTs allowing calibration of the relative gain of each channel. By splitting the emission into two extra beams using two additional polarization-independent beam splitters at near normal incidence, we are able to simultaneously record 4 PMTs (for instance along horizontal, vertical, diagonal, right-circular bases) allowing complete reconstruction of the full Stokes parameters. We also use linearly polarized input light to calibrate the system and confirm that no artifacts are present from the polarization splitting optics. In particular, we confirm that reversing the polarization axes (for instance, swapping H and V) on the detectors, produces exactly equivalent results.

Electronic noise in the detection produces an apparent background polarization magnitude in addition to that contained within the optical signal. Hence even a perfectly polarized input produces a polarization histogram with some deviation about $\rho_l = 0$. For the signal to noise in our measurements this is $\sim 8\%$ and is shown shaded gray in Figs. 2(d) and 3(d).

Using appropriate wave plates we can thus examine the polarization of each pulse along linear (H, V), diagonal ($D, \bar{D}$), and circular (R, L) bases. The fidelity of these measurements is calibrated using the linearly polarized pump laser for different orientations of the input $\lambda/2$ plate, and exceeds 95%. Comparable data from the above-threshold polariton laser [Figs. 2(a) and 2(b)] reveal that each pulse of BEC has a *different* polarization. The intensity of each polarization component is extracted and used to calculate the linear polarization degree [Fig. 2(c)], $\rho_l = (I_H - I_V)/(I_H + I_V)$, with equivalent measures for diagonal (ρ_d) and circular (ρ_c) bases. Repeating the experiment for several hundred pulses in each polarization basis allows construction of a polarization histogram [Fig. 2(d)]. Below threshold, the microcavity emission is unpolarized exhibiting thermal noise around zero absolute polarization. Above threshold, the emission is found to be instantaneously polarized, but with no preferential orientation. The magnitude of the mean polarization is 25% for each basis [given by the standard deviations in Fig. 2(d)], giving a total mean polarization of $\sim 43\%$ just above threshold. The mean

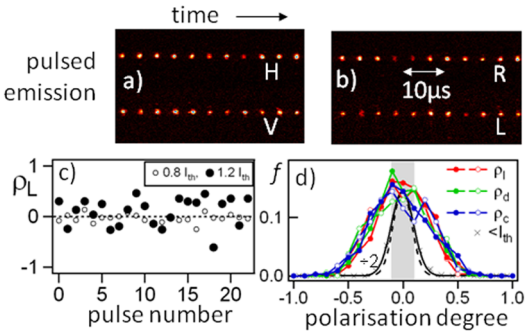

FIG. 2 (color online). Above-threshold polarization-resolved emission when analyzing along (a) horizontal or vertical and (b) right or left circular bases. (c) Extracted linear polarization degree showing stochastic variation from pulse to pulse above and below threshold. (d) Histogram of the fraction of each polarization state f along linear, diagonal, and circular bases of nearly 2000 polariton condensates. Open and closed circles show repeated measurement with reversed polarization split (e.g., H/V and V/H), while crosses show below-threshold unpolarized emission statistics (curve divided by 2 to fit on scale, within detection sensitivity shaded gray and scaled dashed line).

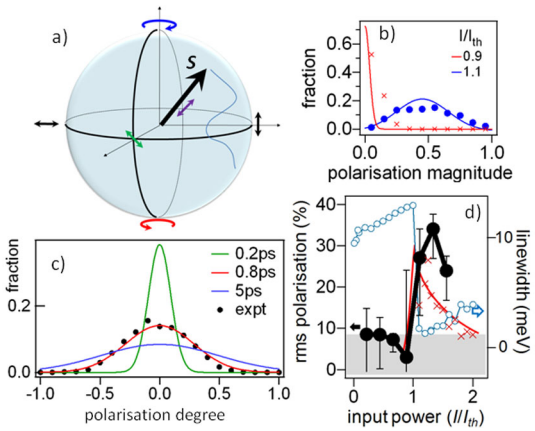

FIG. 3 (color online). (a) Diffusion of the pseudospin, **S** (Stokes polarization vector) of a polariton condensate. (b) Experimental (points) and modeled (lines) histogram of polarization vector lengths, showing shift from zero to ~43% above threshold. (c) Statistical distribution of the linear polarization degree of the condensate showing experiment versus theory for different dephasing times. (d) Root mean square linear polarization degree as a function of pump power (thick black line). Result of theory described in the text (crosses, solid red line is guide to eye) uses linewidth (blue circles) as input parameter.

polarization measured for a single shot is <100% due to the random walk of the polarization vector on a time scale given by the coherence time of the condensate [Fig. 3(a)].

In order to reproduce the experimental polarization histogram, we perform a Monte Carlo simulation of the microcavity emission. At each moment of time the condensate is assumed to be completely polarized but the direction of its pseudospin **S** [see Fig. 3(a)] is initially random. The polarization has a probability to change its direction which is inversely proportional to the dephasing time of the condensate t_i. The coherence time is given by [10] $t_c = (\frac{W_{\text{in}}}{N_0+1} + \frac{1}{t_i})^{-1}$. W_{in} and N_0 are time-dependent and are calculated using the semiclassical Boltzmann equations (3) describing polariton relaxation (see [20]). The dephasing time t_i is governed by the fluctuation of the number of polaritons in the system. For cw pumping $t_i \simeq \frac{\hbar}{V\sqrt{N}}$, where V is the matrix element of interparticle interactions and N is the average number of particles. To simulate the experiment with pulsed excitation, the polarized emission of the ground state is averaged for 100 ps after each pulse and the numerical experiment is repeated 10^5 times.

This model is analogous to the classical Heisenberg spin model [21] used to describe the magnetization in ferromagnets. The spontaneous buildup of polarization is clearly observed above threshold [Fig. 3(b)]. The dephasing time used in the calculation is directly taken from the linewidth measurements [Fig. 3(d)]. Examining the polarization histograms [Fig. 3(c)] shows the best fit is obtained for $t_i = 0.8$ ps (indeed corresponding to the resolution-limited 0.82 meV linewidth). Below threshold, the residual polarization is below the detection limit of our setup, while it increases to a maximum at threshold [Fig. 3(d)] before decreasing again because of the shortening of the dephasing time, due to stronger polariton-polariton interactions [22].

These results thus show that the bosonic exciton polaritons in GaN which form a phase-coherent state above a characteristic density exhibit spontaneous symmetry breaking above 300 K. This contrasts to linear polarization seen in all previous systems (including InP-based bulk vertical cavity surface-emitting lasers [23,24]), and is directly observed through the polarization of light emitted by polaritons. The coherent polariton state thus fulfils all the criteria to be classed as a Bose-Einstein condensate. We stress that these results are completely different from all previous observations in lasers.

This work was supported by EU STIMSCAT, POLAROMA, EPSRC NanoPhotonics Portfolio, and the Swiss National Science Foundation.

[1] A. Imamoglu *et al.*, Phys. Rev. A **53**, 4250 (1996).
[2] H. Deng, G. Weihs, C. Santori, J. Bloch, and Y. Yamamoto, Science **298**, 199 (2002).
[3] Le Si Dang *et al.*, Phys. Rev. Lett. **81**, 3920 (1998).
[4] D. Bajoni *et al.*, Phys. Rev. Lett. **100**, 047401 (2008).
[5] S. Christopoulos *et al.*, Phys. Rev. Lett. **98**, 126405 (2007).
[6] J. Kasprzak *et al.*, Nature (London) **443**, 409 (2006).
[7] R. Balili, V. Hartwell, D. Snoke, L. Pfeiffer, and K. West, Science **316**, 1007 (2007).
[8] C. W. Lai *et al.*, Nature (London) **450**, 529 (2007).
[9] D. Bajoni, P. Senellart, A. Lemaître, and J. Bloch, Phys. Rev. B **76**, 201305 (2007).
[10] F. P. Laussy, I. A. Shelykh, G. Malpuech, and A. Kavokin, Phys. Rev. B **73**, 035315 (2006).
[11] I. A. Shelykh, Yu. G. Rubo, G. Malpuech, D. Solnyshkov, and A. V. Kavokin, Phys. Rev. Lett. **97**, 066402 (2006).
[12] M. Combescot, O. Betbeder-Matibet, and R. Combescot, Phys. Rev. Lett. **99**, 176403 (2007).
[13] J. Goldstone, Nuovo Cimento **19**, 154 (1961).
[14] L. P. Pitaevskii and S. Stringari, *Bose-Einstein Condensation* (Clarendon, Oxford, 2003).
[15] C. N. Yang, Rev. Mod. Phys. **34**, 694 (1962).
[16] Yu. G. Rubo, Phys. Status Solidi A **201**, 641 (2004).
[17] T. Aoki, G. Mohs, M. Kuwata-Gonokami, and A. A. Yamaguchi, Phys. Rev. Lett. **82**, 3108 (1999).
[18] We restrict this analysis to angles below 30° because at higher angles the top Bragg mirror shifts nearly out of resonance. In this pulsed regime, the time-integrated emission intensity at each angle is directly proportional to the polariton occupation at the equivalent in-plane k.
[19] G. Christmann *et al.*, Appl. Phys. Lett. **89**, 261101 (2006).
[20] D. Solnyshkov and G. Malpuech, Superlattices Microstruct. **41**, 279 (2007).
[21] G. S. Joyce, Phys. Rev. **155**, 478 (1967).
[22] D. Porras and C. Tejedor, Phys. Rev. B **67**, 161310 (2003).
[23] R. Sceats *et al.*, Turk. J. Phys. **23**, 781 (1999).
[24] C. J. Hepburn *et al.*, Superlattices Microstruct. **32**, 103 (2002).